# Reflection of circularly polarized light and the effect of particle distribution on circular dichroism in evaporation induced self-assembled cellulose nanocrystal thin films

D. Hewson, P. Vukusic, and S. J. Eichhorn

Citation: AIP Advances **7**, 065308 (2017); doi: 10.1063/1.4986761
View online: https://doi.org/10.1063/1.4986761
View Table of Contents: http://aip.scitation.org/toc/adv/7/6
Published by the American Institute of Physics

# Reflection of circularly polarized light and the effect of particle distribution on circular dichroism in evaporation induced self-assembled cellulose nanocrystal thin films

D. Hewson,[1] P. Vukusic,[1] and S. J. Eichhorn[2,a]
[1]*College of Engineering, Mathematics and Physical Sciences, Physics Building, North Park Road, University of Exeter, Exeter EX4 4QL, United Kingdom*
[2]*College of Engineering, Mathematics and Physical Sciences, Harrison Building, Stocker Road, University of Exeter, Exeter EX4 4QF, United Kingdom*

(Received 29 March 2017; accepted 6 June 2017; published online 14 June 2017)

Evaporation induced self-assembled (EISA) thin films of cellulose nanocrystals (CNCs) have shown great potential for displaying structural colour across the visible spectrum. They are believed primarily to reflect left handed circularly polarised (LCP) light due to their natural tendency to form structures comprising left handed chirality. Accordingly the fabrication of homogenously coloured CNC thin films is challenging. Deposition of solid material towards the edge of a dried droplet, via the coffee-stain effect, is one such difficulty in achieving homogenous colour across CNC films. These effects are most easily observed in films prepared from droplets where observable reflection of visible light is localised around the edge of the dry film. We report here, the observation of both left and right hand circularly polarised (LCP/RCP) light in reflection from distinct separate regions of CNC EISA thin films and we elucidate how these reflections are dependent on the distribution of CNC material within the EISA thin film. Optical models of reflection are presented which are based on structures revealed using high resolution transmission electron microscopy (TEM) images of film cross sections. We have also employed spectroscopic characterisation techniques to evaluate the distribution of solid CNC material within a selection of CNC EISA thin films and we have correlated this distribution with polarised light spectra collected from each film. We conclude that film regions from which RCP light was reflected were associated with lower CNC concentrations and thicker film regions.  [http://dx.doi.org/10.1063/1.4986761]

The mechanical properties of cellulose that give plants their structural integrity have been exploited in useful materials e.g. paper and fibre yarns. Cellulose nanocrystals (CNCs), extracted from plant cell walls by acid hydrolysis possess excellent mechanical, thermal and electrical properties that lend themselves to potential products.[1–4] CNC suspensions are known to exhibit interesting optical properties,[5–7] self-assemble in confinement[6–8] and display coloration in flexible and shape memory films.[8–10] Such properties are derived from nematic liquid crystalline phases of the rod-like CNCs that have intrinsic right handed twist[11,12] and self-assemble in solution below specific concentrations. The nematic ordering of CNCs undergoes chiral twisting to form chiral nematic or cholesteric structures[13,14] which possess a left handed twist.[15–17] Chiral nematic structures possess optical properties that include circular dichroism, pseudo-Bragg reflections and strong rotatory power.[18] These properties are observed in solutions of CNCs from which the structures responsible for them can be frozen in upon evaporation of the solvent in a process called evaporation induced

[a]Electronic mail: s.j.eichhorn@exeter.ac.uk

 

self-assembly (EISA). These iridescent films offer a unique way of generating visible color using a renewable and sustainable material.[19] Drying droplets comprising suspended nanoparticles, give rise to a characteristic ring-like deposit found along the perimeter of the drop.[20] Drying droplets provide a replenishment of water from the interior of the drop to the edges where evaporation occurs more readily, creating a net flow of water outwards that carries solid material to the edge of the drying droplet. Peiss *et al.* showed that the relationship between the rate of evaporation and the radius of drying drops is non-linear.[21] This property probably contributes to the inhomogeneous distribution of solid material within EISA films and may help to explain variations in optical behaviour.[22] We report optical variations observed in CNC thin films that include the reflection of both left and right hand circularly polarised (LCP/RCP) light from distinct separate regions of CNC EISA thin films. Our TEM analysis of CNC film micro-structures intended to elucidate how this reflection is dependent on the distribution of CNC material within the films, relating the structures observed to inherent optical properties. Unable to achieve our goal by directly using TEM, we have employed spectroscopic techniques to evaluate the distribution of CNC material within a range of thin films, correlating this distribution with polarised light spectra. This is a new approach to the characterisation of dried aqueous droplets of CNCs within dried thin films, useful for understanding how variations in film structure correlate with optical properties.

A 6 wt. % aqueous solution of CNCs was obtained from FP Innovations. The CNCs have a sulphur content of 0.7-0.8% of the CNC mass and NaOH counter ions were used in CNC synthesis. CNC droplets (10μl) were cast onto glass slides and weighed. The droplets were left to dry at ambient temperature and pressure. The reflection of unpolarised, LCP and RCP light from dried films was recorded using microspectrophotometry (MSP) in a Zeiss Axioskop2 microscope fitted with circular polarising filters. Incident light was delivered via an optical fibre while reflected light was collected using another optical fibre connected to an Ocean Optics USB2000+ spectrometer. Samples were mounted on a micrometer stage onto which the film substrate was attached and could be moved within the *x-y* plane to within 2μm. The CNC film presented in Figure 1a was investigated using polarised optical microscopy, close-up images of which are presented in Figure 1b–c where the reflection of LCP light is seen in a narrow strip around the edge of the film (Fig. 1b). Within this reflection strip are bands of color which are orange at the edge of the film and blue-shift across the strip to violet. The color reflection diminishes in intensity approximately 200 μm from the edge of the film. The reflection of RCP light is seen in a similarly narrow strip adjacent to and inside the LCP region (Fig. 1c). This strip is similar in width but presents a narrower band of color. The bands are separate and distinct; this is confirmed by the MSP data taken from the same section of film using LCP and RCP filters (Fig. 1d–e). The data in Figure 1d–e highlight the comparable intensities of reflection from each region and the difference in the range and degree of color and blue-shift in each. Spectra obtained from regions within each LCP and RCP reflecting strip (Fig. 1f and i) show complimentary color transmission of RCP and LCP. The strip where LCP light is reflected transmits RCP light (Fig. 1g–h) while the strip reflecting RCP light itself transmits LCP light (Fig. 1j–k). The complimentary reflection/transmission data might suggest the presence of a right handed chiral structure and that the film changes from a left handed chiral structure at the edge to a right handed chiral structure further in. Although complimentary reflection/transmission was measured at specific points within each region, TEM confirmation was required to confirm the presence of right handed chiral structures.

TEM samples of cross-sections were prepared using a method used by Giasson.[23] A TEM image of a section through a complete edge of a CNC thin film is shown in Figure 2a, with subsequent close-ups in Figure 2b–c. These images show a relatively uniform and homogenous chiral structure (Fig 2a–c) throughout the length of the section, in agreement with the SEM investigation of Park *et al.*[24] A TEM image of an oblique cut is shown in Figure 2c. No features were observed that could obviously give rise to RCP reflections. The curved features in these images, known as Bouligand curves that are associated with chiral structures, were all found to 'arc' in the same direction. No unidirectional layer was observed within the helicoidal regions, as has been observed in certain beetle integument, where it exhibits half-wave retarding properties.[25] Defects in the layered structure (Fig.2 d–f) were however observed, and are consistent with the observations of Wang *et al.*[15] These defects form phase boundaries, created after the formation of tactoids during the initial self-assembly process which then fuse to form the overall film.[15]

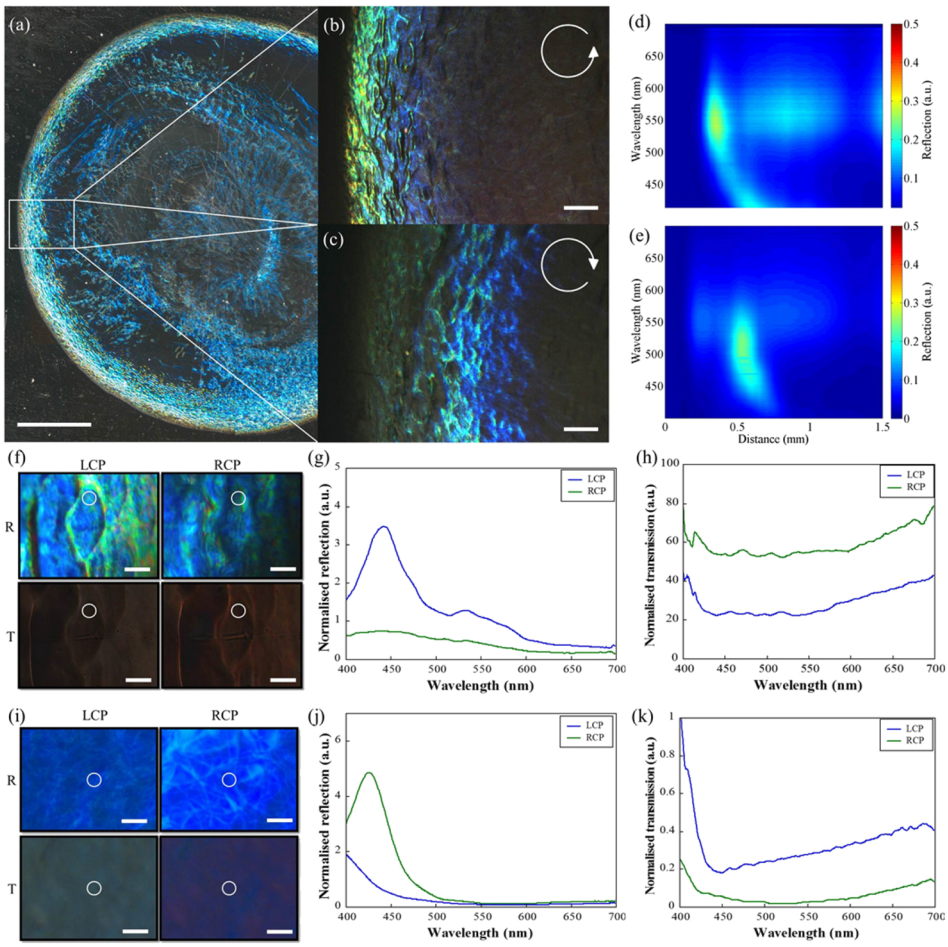


FIG. 1. (a). Typical unpolarised dark field image of the CNC film. (b-c). Typical bright field images of the same film region using LCP and RCP analysers. (d-e) Typical color maps showing reflection of LCP and RCP respectively as a function of distance along the film. (f) Optical microscope images of the same area of the film observed through LCP and RCP filters using a x50 objective lens (numerical aperture 0.5) in reflection and transmission. The area of the film was within the region reflecting LCP light. The circle marks the location of the beam spot. (g-h) LCP and RCP light reflection and transmission spectra taken from the area marked in (f). (i) Optical microscope images of the same area of the film observed through LCP and RCP filters in reflection and transmission. The area of the film was within the region reflecting RCP light. (j-k) LCP and RCP light reflection and transmission spectra taken from the area marked in (i). Scale bars (a) 1 mm, (b-c) 100 μm, (f and i) 20 μm.

We observed defects in this region that could be responsible for the reflection of RCP light, but they were small in relation to the size of the imaged area, and not clustered enough in this region to alter the reflected light appreciably. We note the recently published work by Wilts *et al.*[17] that describes the RCP reflection in films of CNCs is weak at low angles, but comparatively high at larger angles. It could also therefore be some artefact of the optical set up and curvature of the droplet that enhances the RCP reflections observed in our samples. Small variations in pitch length were observed from measurements taken along z-axis (through thickness) (supplementary material, Fig. 1Sa) which were used to model the reflection of visible light. Pitch lengths were observed to vary, being shorter at the bottom of the film and longer at the top. Reflection measurements matched theoretical modelling of reflectance of both LCP and non-polarised light from the films (supplementary material, Fig. 1Sb and c). The reflection of RCP light remains unexplained as no evidence could be discerned in the TEM cross-sections for a structure that would produce such an effect. Spectroscopic measurements using a goniometer reflection measurement setup were used to explore the angle dependence of the reflection of LCP and RCP light. The data presented in supplementary material, Figure 1Sd shows that for incident angles 10-60° the optical behaviour for LCP and RCP light follow a similar monotonic decrease with increasing incident angle.

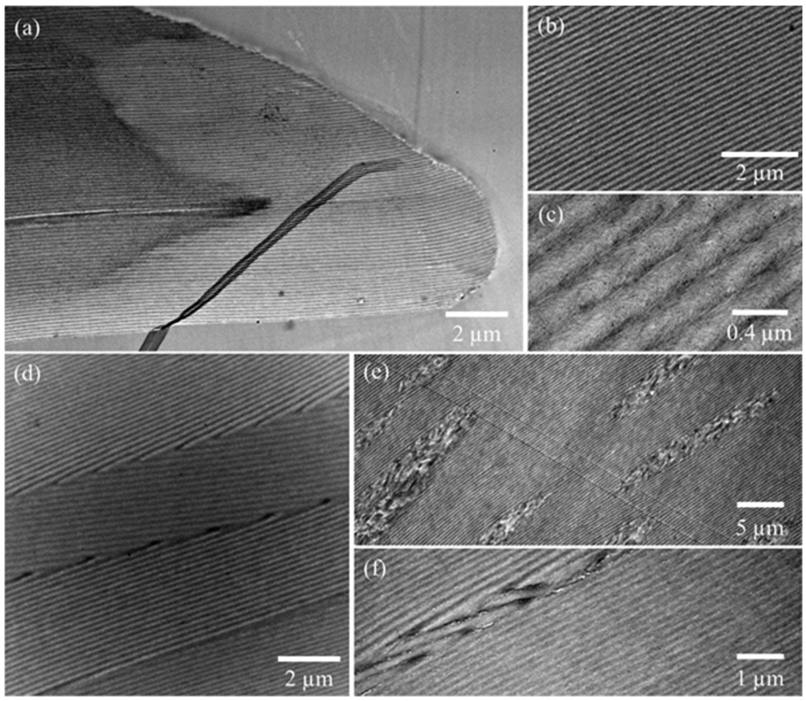


FIG. 2. TEM images showing CNC film cross-sections. (a). The edge of a CNC film with visible multilayer structure. The dark ribbon is where the film has folded during sample preparation. (b-c). Magnifications of the multilayer structure where, in (c), the Bouligand curvature is visible. (d-f). Images showing fusion defects in the multilayer structure.

As the reflection of RCP could not be explained by the more conventional methods the following approach was developed. This involved combining film dimensions with spectroscopic techniques to obtain information about the distribution of CNCs along a given line spanning a diameter of a film. The distribution was calculated as a relative concentration value using spectroscopic measurements of reflection and transmission. These measurements were taken using the MSP set-up described above. Calculations of the nanocrystal distribution required knowledge of the volume of the section of film under investigation and the mass of solid material within the section. Details of this calculation are contained within supplementary material.

The average length and width of an individual CNC was 108 nm × 6 nm (with respective standard deviations of 34.5 nm and 1.9 nm), found from TEM images (supplementary material, Fig. 2Sa). The volume and mass (assuming a density of 1.5 g $cm^{-3}$) of a single CNC ($V_{CNC}$ and $m_{CNC}$) were calculated at $388.8\times10^{-20}$ $cm^3$ and $5.8\times10^{-18}$ g respectively. With a known mass of a single CNC the total number ($N$) of CNCs in a film was calculated using the equation $N = m/m_{CNC}$, where $m$ is the mass of the film which is 6 wt.% of the cast droplet. The volume of the film ($V$) is then obtained by multiplying $N$ by the volume of individual nanocrystals. So, $NV_{CNC} = V$. The mass of the solid content and the theoretical volume were calculated to be 0.654 mg and $436\times10^6$ $\mu m^3$. The volumes calculated using an average area and individual areas were $483.1\times10^6$ $\mu m^3$ ± 0.0016% and $483.3\times10^6$ $\mu m^3$ ± 0.0016%. Values for additional films measured are presented in Table 1S in the supplementary material. The spectroscopic data show no correlation between film height and the reflection of visible light. Non-polarised light was used to take reflection and transmission spectra across the diameter of the film (supplementary material, Fig. 2Sa). Absorbance was then calculated for a number of points and used to correlate with the known mass within the volume of the film. A distribution profile is presented in Figure 3a along with the film profile. CNC concentrations are significantly higher at the edge of the film where a CNC concentration of 27.7 g $cm^{-3}$ rapidly decreases to 2.4 g $cm^{-3}$ and then undergoes an incremental decrease to reach a plateau at ~0.7 g $cm^{-3}$. The dashed lines in Figure 3a highlight the color transitions from the edge inwards. Colors at the red end of the visible spectrum are observed in the first band (up to the first dashed line). This then transitions to yellow and green colors in the middle band. In the broadest section, between the last two dashed lines, blue and purple

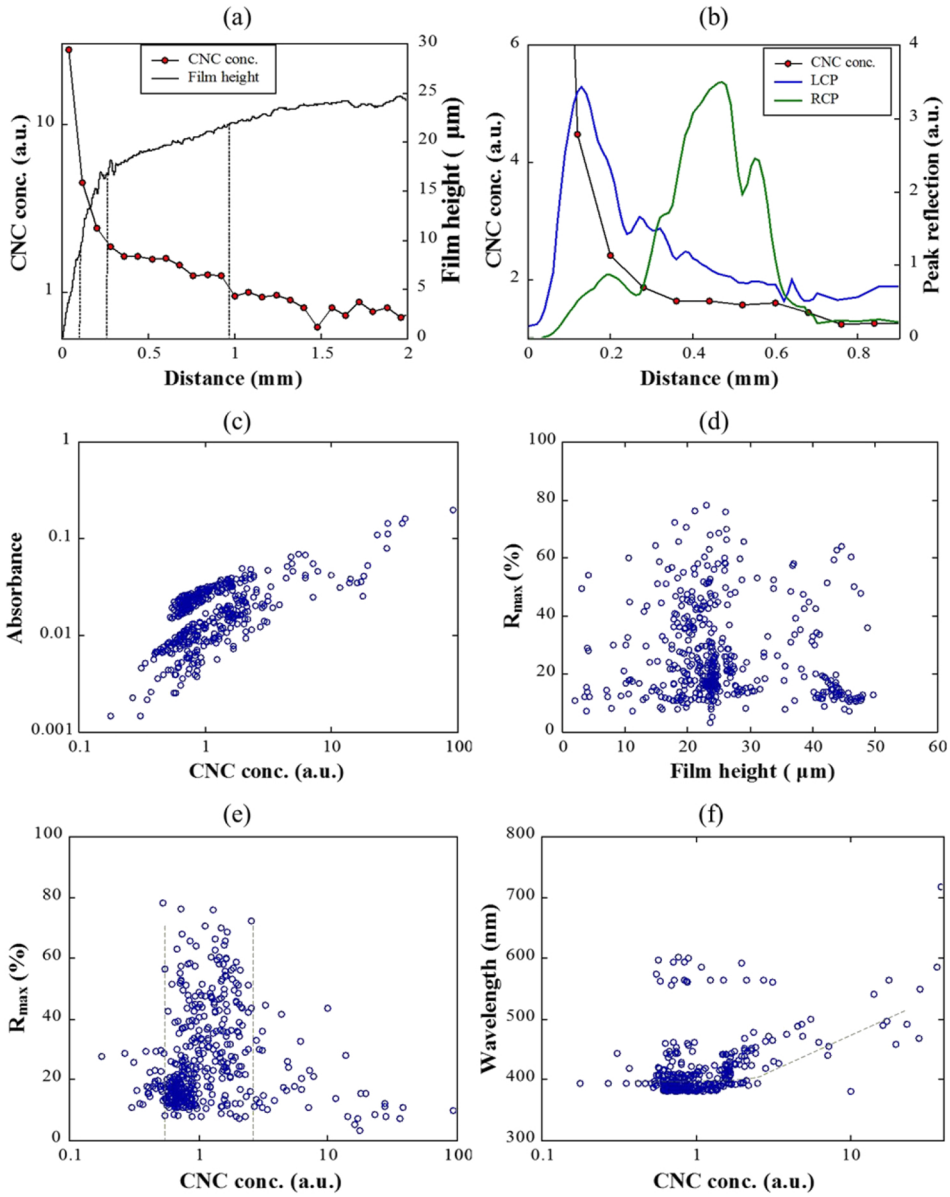


FIG. 3. (a) Log plot of CNC concentration shown with film profile as a function of distance. Dashed lines indicate a color transition. (b) Highlighted section of the CNC concentration shown with the peak reflection of LCP and RCP light along the film profile shown in (a). (c) Log plot of absorbance normalised to the film height as a function of CNC concentration. (d-e) Log plots of peak reflection ($R_{max}$) as a function of film height and CNC concentration. The dashed lines highlight the region in (e) where $R_{max}$ is higher within a narrow concentration band. (f) Log plot of wavelengths of reflected light as a function of CNC concentration. The dashed line highlights the red-shift in reflected wavelength with increasing concentration.

colors are observed up to the final dashed line after which no more color is observed. When the CNC concentration is plotted against the peak reflection of both LCP and RCP light (Figure 3b) a distinct change in CNC concentration is observed from where each polarization is reflected. LCP light is strongly reflected from regions of higher CNC concentration and RCP light from regions of lower CNC concentration.

Peak intensity reflection values were not observed from the thickest film regions; a decrease in reflection with increasing film height was observed instead. Overall, the results indicate that film height has little effect on the reflection of visible light. Figure 3c shows that the absorbance (normalised to the film height) monotonically increases with increasing CNC concentration. The peak reflection values in Figure 3d show no correlation between reflection and film height.The majority

of the reflected light, however seems to occur at a film height of 25 μm, approximately half the maximum film height. The highest intensity reflections also occur at this film height. A similar but more pronounced column of data is observed in Figure 3e where peak reflections occur within a narrow CNC concentration band (highlighted by the vertical dashed lines). Figure 3f shows the reflected wavelengths, for the same films, as a function of CNC concentration. Two bands are seen, a narrow band at ~580 nm and a slightly broader band located at ~400 nm. As the CNC concentration increases the band located at ~400 nm red shifts and the narrow band at ~580 nm disappears. Both these transitions are directly correlated with a change in the concentration of CNCs, thereby providing a link between optical and structural properties. The question of what is responsible for RCP light reflection remains unanswered. Spectroscopic techniques and polarised microscopy have confirmed that there is a significant reflection of RCP light but TEM investigations have failed to provide any discernible indication as to the structures responsible. Our investigation into CNC distribution has shown that progressing from the edge of the film towards the centre the CNC concentration decrease and the film height increases. One possibility is that defects are being introduced because of the lower concentration of CNCs in regions of greater thickness, leading to disclinations of tactoids during sedimentation.

## CONCLUSION

Optical measurements showing significant reflection of both LCP and RCP light from CNC thin films have been presented, but while TEM analysis has revealed the structures responsible for the reflection of LCP light, the structures responsible for the reflection of RCP light remain elusive. The volume of thin films of dried cellulose nanocrystals has been calculated theoretically and experimentally. The calculated volumes have been used in conjunction with optical measurements to evaluate the distribution of CNCs along the diameter of the films. A difference in the nanocrystal concentration has been shown to exist between regions expressing a significant difference in reflection of either LCP or RCP light. Right handed circularly polarised light is shown to occur in a region of the film of low nanocrystal concentration and greater film height.

## SUPPLEMENTARY MATERIAL

See supplementary material for a table showing the mass of CNCs in each film and the theoretical and calculated volumes of the dry films (Table 1S), data on the variation of pitch lengths (Figure 1S) and the calculation of CNC concentration including the dimensions of the materials (Figure 2S).

## ACKNOWLEDGMENTS

The authors would like to thank the University of Exeter for providing funding for a doctoral studentship.

[1] S. J. Eichhorn, Soft Matter **7**, 303 (2011).
[2] Y. Habibi, L. A. Lucia, and O. J. Rojas, Chemical Reviews **110**(6), 3479 (2010).
[3] N. Lavoine, I. Desloges, A. Dufresne, and J. Bras, Carbohydrate Polymers **90**(2), 735 (2012).
[4] P. Podsiadlo, L. Sui, Y. Elkasabi et al., Langmuir **23**(15), 7901 (2007).
[5] A. Haywood and V. Davies, Cellulose **24** (2017).
[6] J. F. Revol, H. Bradford, J. Giasson, R. H. Marchessault, and D. G. Gray, International Journal of Biological Macromolecules **14**(3), 170 (1992).
[7] D. Liu, S. Wang, Z. Ma et al., RSC Adv. **4**(74), 39322 (2014).
[8] M. Tatsumi, Y. Teramoto, and Y. Nishio, Cellulose **22**(5), 2983 (2015).
[9] R. M. Parker, B. Frka-Petesic, G. Guidetti, G. Kamita, G. Consani, C. Abell, and S. Vignolini, ACS Nano **10**(9), 8443 (2016).
[10] G. Guidetti, S. Atifi, S. Vignolini, and W. Y. Hamad, Advanced Materials **28**(45), 10042 (2016).
[11] A. Espinha, G. Guidetti, M. C. Serrano, B. Frka-Petesic, A. G. Dumanli, W. Y. Hamad, A. Blanco, C. Lopez, and S. Vignolini, ACS Applied Materials & Interfaces **8**(46), 31935 (2016).
[12] K. Conley, M. A. Whitehead, and T. G. M. van de Ven, Cellulose **24**(2), 479 (2017).
[13] I. Usov, G. Nystrom, J. Adamcik, S. Handschin, C. Schutz, A. Fall, L. Bergstrom, and R. Mezzenga, Nat. Commun. **6** (2015).
[14] J. P. F. Lagerwall, C. Schutz, M. Salajkova, J. Noh, J. H. Park, G. Scalia, and L. Bergstrom, NPG Asia Materials **6** (2014).

[15] P. X. Wang, W. Y. Hamad, and M. J. MacLachlan, Nat. Commun. **7** (2016).
[16] J. Majoinen, E. Kontturi, O. Ikkala, and D. G. Gray, Cellulose **19**(5), 1599 (2012).
[17] B. Wilts, A. Dumanli, R. Middleton, P. Vukusic, and S. Vignolini, APL Photonics **2**(4), (2017).
[18] H. Devries, Acta Crystallographica **4**(3), 219 (1951).
[19] A. G. Dumanli, H. M. van der Kooij, G. Kamita, E. Reisner, J. J. Baumberg, U. Steiner, and S. Vignolini, ACS Applied Materials & Interfaces **6**(15), 12302 (2014).
[20] R. D. Deegan, O. Bakajin, T. F. Dupont, G. Huber, S. R. Nagel, and T. A. Witten, Nature **389**(6653), 827 (1997).
[21] C. N. Peiss, Journal of Applied Physics **65**(12), 5235 (1989).
[22] X. Y. Mu and D. G. Gray, Cellulose **22**(2), 1103 (2015).
[23] J. Giasson, J. F. Revol, A. M. Ritcey, and D. G. Gray, Biopolymers **27**(12), 1999 (1988).
[24] J. H. Park, J. Noh, C. Schutz, G. Salazar-Alvarez, G. Scalia, L. Bergstrom, and J. P. F. Lagerwall, Chemphyschem **15**(7), 1477 (2014).
[25] S. Caveney, Proceedings of the Royal Society Series B-Biological Sciences **178**(1051), 205 (1971).